Laser and Particle Beams (2012), *30*, 39–43.

doi:10.1017/S0263034611000668

Directional transport of fast electrons at the front target surface irradiated by intense femtosecond laser pulses with preformed plasma

X.X. LIN,[1] Y.T. LI,[1] B.C. LIU,[1,2,3] F. LIU,[1] F. DU,[1] S.J. WANG,[1] L.M. CHEN,[1] L. ZHANG,[1] X. LIU,[1] X.L. LIU,[1] Z.H. WANG,[1] J.L. MA,[1] X. LU,[1] Q.L. DONG,[1] W.M. WANG,[1] Z.M. SHENG,[1] Z.Y. WEI,[1] AND J. ZHANG[1,4]

[1]Beijing National Laboratory for Condensed Matter Physics, Institute of Physics, Chinese Academy of Sciences, Beijing, China
[2]State Key Laboratory of Nuclear Physics and Technology, Peking University, Beijing, China
[3]Graduate University of the Chinese Academy of Sciences, Beijing, China
[4]Shanghai Jiao Tong University, Shanghai, China

(RECEIVED 27 January 2011; ACCEPTED 8 October 2011)

Abstract

The effects of laser incidence angle on lateral fast electron transport at front target surface, when a plasma is preformed, irradiated by intense ($>10^{18}$ W/cm^2) laser pulses, are studied by K_α imaging technique and electron spectrometer. A horizontally asymmetric K_α halo, resulting from directional lateral electron transport and energy deposition, is observed for a large incidence angle (70°). Moreover, a group of MeV high energy electrons is emitted along target surface. It is believed that the deformed preplasma and the asymmetrical distribution of self-generated magnetic field, at large incidence angle, play an important role in the directional lateral electron transport.

Keywords: Electron energy spectra; Fast electron transport; K_α x-ray imaging; Laser-plasma interactions

INTRODUCTION

The lateral fast electron transport at the target surface irradiated by intense laser pulses has attracted great attention because of the important role it plays in the cone guided scheme for fast ignition of inertial confinement fusion (Kodama *et al.*, 2001). Theoretical works have shown that the conical target can both guide the laser light and the fast electrons to the tip of the cone, which leads to an enhancement of the fast electron density near the cone tip (Sentoku *et al.*, 2004; Nakamura *et al.*, 2004). Li *et al.* (2006*b*) and Habara *et al.* (2006) have experimentally observed the fast electron beam emitting along the target surface into vacuum when the laser incidence angle is large. The observation of fast electrons transporting inside the conical target with K_α imaging technique does not show obvious fast electron current along the inner wall of the conical target and the enhancement of the energy deposition near the cone tip. It is believed that the preplasma filling inside the cone, created by the prepulse and the pedestal of the intense laser pulse, inhibits the fast electron transport to the cone tip (Baton *et al.*, 2008; Van Woerkom *et al.*, 2008). Recently, the K_α imaging measurement of a simple planar target foil with a preplasma irradiated by intense femtosecond (fs) laser pulses indicates that the fast electrons can laterally drift in the preplasma and deposit energy far away from the focal spot, due to the self-generated electrostatic field (E field) and magnetic field (B field) generated by the non-collinear gradients of electron temperature and density (Yabuuchi *et al.*, 2010; Lin *et al.*, 2010).

In this work, the lateral fast electron transport at the front target surface of a planar Cu foil as a function of laser incidence angle, when a preplasma is formed, is studied by K_α imaging technique and electron spectrometer. When the incidence angle is 70°, a horizontally asymmetric K_α halo structure is observed, corresponding to directional lateral fast electron transport and energy deposition at front target surface. Furthermore, the surface fast electron spectrum has a high energy tail with an electron temperature $T_{hot} \sim 1.6$ MeV, which is much higher than the 45° case. It is believed that the deformation of the preplasma and the spatial

Address correspondence and reprint requests: Y.T. Li, Beijing National Laboratory for Condensed Matter Physics, Institute of Physics, Chinese Academy of Sciences, Beijing 100190, China. E-mail: ytli@aphy.iphy.ac.cn

distribution of the self-generated magnetic field are responsible for the directional lateral electron transport.

EXPERIMENTAL SETUP

The experiments were performed at the Institute of Physics, Chinese Academy of Sciences, using the Xtreme Light II (XL-II) Ti: sapphire laser system, which can deliver a linearly-polarized pulse with energy up to 0.6 J in 60 fs at 800 nm (Zhang *et al.*, 2005). The *p*-polarized laser pulse was focused onto a 50 μm thick Cu foil target at incidence angle of 45° or 70° with an $f/3.5$ off-axis parabolic mirror. The diameter of the focal spot was about 4.5 μm at the full width at half maximum, in which contained about 35% of the laser energy. The laser intensity was up to 5×10^{18} W/cm^2. The amplified spontaneous emission (ASE) was measured to be about 10^{-5} at about 10 ps before the peak of the main pulse. A prepulse, split from the main pulse, with similar focal spot to that of the main pulse, was used to generate a preplasma. The intensity of the prepulse was about 10^{16} W/cm^2. The delay time, Δt, between the prepulse and the main pulse was about 0.6 ns.

Spherically bent quartz 2131 crystal was used to image the Cu K_α emission at 8.048 keV onto a 16 bit charge-coupled device with a magnification of about 8. The radius of curvature of the crystal was 380 mm. A 30 mm diameter aperture was put in front of the crystal, giving an astigmatism-limited spatial resolution about 19 μm (Koch *et al.*, 2003). The energy bandwidth was about 11 eV (Akli *et al.*, 2007). The crystal viewed the K_α emission at an angle of 48° with respect to the front target normal. A calibrated electron magnetic spectrometer with 1000 G permanent magnets was used to measure the energy spectrum of the out-going electrons at about 10° with respect to the front target surface.

RESULTS AND DISCUSSIONS

Figures 1a and 1b show the typical K_α images taken for laser incidence angle of 45° and 70°, respectively. The laser pulse is incident from the left in the images. The energy of the main laser pulse is about 280 mJ for the two cases.

Several features can be seen from the images. A large K_α halo structure surrounding the central spot is observed for both cases. This halo, which has been investigated in our previous work (Lin *et al.*, 2010), is mainly excited by the fast electrons laterally transporting in the self-generated *E* and *B* fields in the preplasma and depositing energy far away from the central focal spot. The most striking feature in Figure 1 is that the pattern of the halo is dependent on the laser incidence angle, θ. When θ is 45°, the halo is almost symmetrically distributed surrounding the central spot, with a radius of about 160 μm. In contrast, for the 70° case, the halo becomes asymmetric in the horizontal direction. The size of the right side of the halo reaches about 320 μm, which is about two times larger than the left side and that of the 45° case.

Figure 2 shows the energy spectra of fast electrons emitted into vacuum close to the direction parallel to the target surface, when θ is 45° and 70°, respectively. The electron spectra are fitted by the exponential distribution function (Li *et al.*, 2001), to estimate the fast electron temperature T_{hot}. For the 45° case, T_{hot} is 276 keV, which is close to the value by Beg's (1997) scaling. For the 70° case, the electron spectrum shows a two-temperature structure, with a lower T_{hot} of 277 keV, and a higher T_{hot} of 1.6 MeV.

In previous work (Lin *et al.*, 2010), we identified the origin of the K_α halo structure experimentally, by using a "step-like" target. When the prepulse arrives at the target surface, a preplasma is generated. The following ASE continually heats the expanding preplasma. Due to the non-collinear gradients of electron temperature and density $\nabla T_e \times \nabla n_e$ (Stamper *et al.*, 1971), a toroidal thermoelectric *B* field can be generated in the preplasma. The *B* field concentrates on the boundary of the preplasma and expands with the plasma bubble (Stamper *et al.*, 1978; Li *et al.*, 2009). In addition, an *E* field can be established due to the space charge separation (Wallace, 1985; Mora & Pellat, 1979). During the interaction of the fs main pulse with the preplasma, fast electrons are produced near the critical density surface via collisionless absorption mechanisms (Gibbon & Forster, 1996). After a complex lateral drift in the *E* and *B* fields, a group of these fast electrons deposit their energy

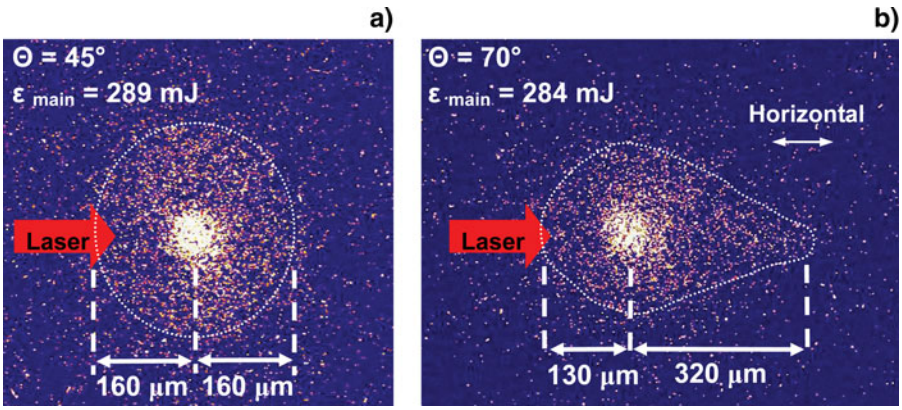

Fig. 1. (Color online) Typical K_α images taken at the laser incidence angle of (**a**) 45° and (**b**) 70°. ε_{main} is the main laser energy, θ is the laser incidence angle. The laser is incident from the left.

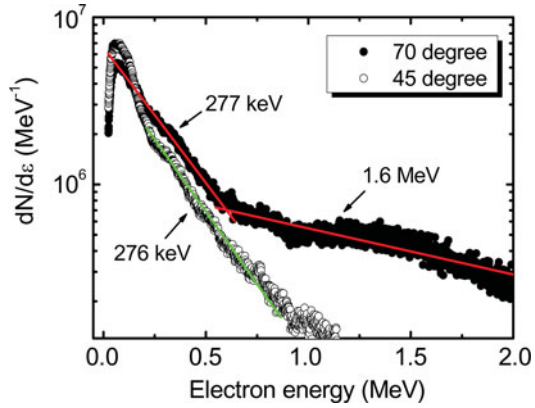

Fig. 2. (Color online) Electron energy spectra detected by the magnetic spectrometer at about 10° with respect to the front target surface, when the incidence angle is 45° (open circle) and 70° (solid circle), respectively.

far away from the focal spot and excite the K_α halo emission structure (Lin *et al.*, 2010).

Three possibilities may cause the asymmetry of the K_α halo when the laser incidence angle is large. The first is the laterally transported fast electron current confined and guided by the surface E and B fields as a current along the initial target surface, which may excite a prolonged K_α emission region on the right side of the focal spot (the side of the reflected laser). However, this surface current of fast electrons is significant only when the plasma density profile is steep enough (Li *et al.*, 2006*b*; Chen *et al.*, 2006*b*; Ma *et al.*, 2006). The second is the prolonged geometrical laser focal spot at large incidence angle. However, this geometrical extension is far smaller than the size of the asymmetrical halo. The third possibility is the deformation of the preplasma due to the grazing incidence of the laser pulse, which can push the plasma toward the laser propagation direction due to the ponderomotive force. This may leads to an asymmetric spatial distribution of the self-generated B field, which can significantly influence the trajectories of the fast electrons laterally drifting in the plasma above the initial target surface.

The effect of the ponderomotive force on the deformation of preplasma can be roughly estimated. The velocity of the plasma element, pushed by the laser ponderomotive force, can be estimated as (Wilks *et al.*, 1992):

$$u = c\left[\frac{n_{cr}}{2n_e}\frac{Zm_e}{m_i}\frac{I\lambda_\mu^2}{1.37\times 10^{18}}\right]^{1/2}, \tag{1}$$

where c is velocity of light; n_{cr} is plasma critical density; n_e is plasma density; Z is ion charge; m_e and m_i are electron mass and ion mass, respectively; I is laser intensity in W/cm^2, and λ_μ is laser wavelength in μm. Considering the average contribution of the 10 ps pedestal rising edge before the main peak, taking preplasma density $n_e \sim 10^{19}$ cm^{-3}, and the average $I\lambda_\mu^2 \sim 6.4\times 10^{16}$ W/cm^2, Eq. (1) gives $u \sim 0.024c = 7.2$ μm/ps. Therefore, the grazing incident laser pulse can push the preplasma boundary horizontally by about 70 μm in 10 ps before the main peak arrives.

To illustrate this deformation effect of preplasma on the lateral fast electron transport, we perform a two-dimensional relativistic simulation of the fast electron trajectories in specified E and B fields schematically. According to previous results (Stamper *et al.*, 1978; Li *et al.*, 2009), the B field spatial distribution $B_\theta(r,z)$ is parametrized by

$$B_\theta(r,z) = -B_{\max}(r^2/{a_0}^2 + z^2/{b_0}^2)(r/\sqrt{z^2+r^2}),$$

for

$$(r^2/{a_0}^2 + z^2/{b_0}^2) < 1, \tag{2a}$$

$$B_{\theta(r,z)} = -B_{\max}(r^2/{a_0}^2 + z^2/{b_0}^2)^{-1}(r/\sqrt{z^2+r^2}),\ \text{for}\ 1 < (r^2/{a_0}^2 + z^2/{b_0}^2)\ \text{and}\ (r^2/{a_1}^2 + z^2/{b_1}^2) < 1, \tag{2b}$$

$B_\theta\,(r,z) = 0$, for

$$(r^2/{a_1}^2 + z^2/{b_1}^2) > 1, \tag{2c}$$

where r and z are the coordinates of the two-dimensional space, $z = 0$ surface is set to be the initial target surface; B_{max} is the maximum strength of the B field; a_0, b_0 are the semi-major and semi-minor axis of the ellipsoid shell where the B field is maximum; a_1, b_1 are the semi-major and semi-minor axis of the ellipsoid shell assumed to be the outer boundary of the B field region. The toroidal B field is in the minus theta direction. The electron trajectories on the right side of the central spot ($r > 0$) are simulated with incidence angle of 45° and 70°. For 45° case, a_0 and b_0 are set to be equal to 50 μm, a_1 and b_1 are set to be 75 μm. Thus the B field is concentrated around a spherical shell, to simulate the symmetric preplasma bubble for the 45° case. For 70° case, a_0 and b_0 are set to be 100 and 50 μm, a_1 and b_1 are set to be 150 and 75 μm, respectively. Thus the B field is concentrated around an *ellipsoid* shell, which originates from the asymmetrical distribution of the gradients of the electron temperature and density of the deformed preplasma. Figures 3a and 3b show the constructed B field distribution on the right side of the focal spot for 45° and 70°, respectively. The B_{max} is set to be 0.5 MG (Stamper *et al.*, 1971, 1978; Li *et al.*, 2009) both for the two cases. For simplification, the E field is set to be a fixed strength of $E_z \sim 1\times 10^9$ V/m in the z direction (Wallace, 1985; Li *et al.*, 2006*a*). The fast electrons with different initial kinetic energy, are launched near the assumed critical surface ($r \sim 0$ and $z \sim 15$ μm) with the emission direction of the specular laser light (Sentoku *et al.*, 1999; Sheng *et al.*, 2000; Chen *et al.*, 2006*a*).

Figures 3c and 3d show the fast electron trajectories on the right side of the central spot calculated for the 45° and 70°

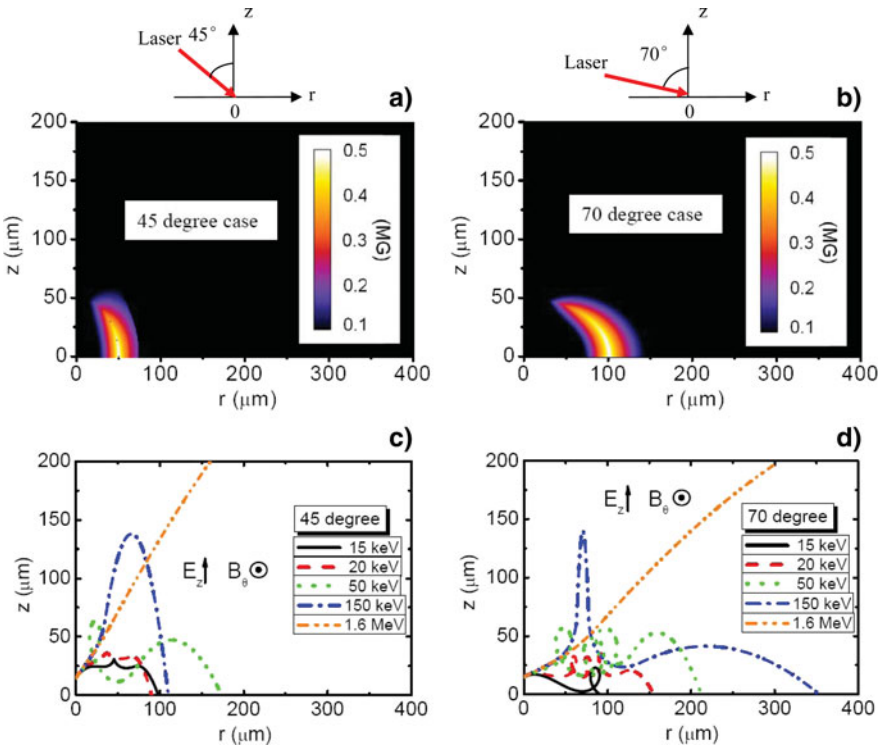

Fig. 3. (Color online) (**a**) *B* field distribution according to Eq. (1), when B_{max} is 0.5 MG, a_0 and b_0 are 50 μm, a_1 and b_1 are 75 μm. (**b**) *B* field distribution when B_{max}, a_0, b_0, a_1, and b_1 are 0.5 MG, 100 μm, 50 μm, 150 μm, and 75 μm, respectively. (**c**) and (**d**) show the corresponding fast electron trajectories calculated with the *B* field distribution shown in (a) and (b), respectively. The initial kinetic energy of the fast electrons is changed from 15 keV to 1.6 MeV.

cases, respectively. For the 70° case, due to the larger extension of the *B* field in the *r* direction and the larger initial electron launch angle with respect to the normal axis, the fast electrons can drift a longer distance laterally in the *E* and *B* fields, and deposit their energy further away from the central spot than the 45° case. This can explain the prolonged K_α halo structure on the right side of the central spot shown in Figure 1b. Furthermore, for the 70° case, high energy (MeV level) fast electrons can emit into vacuum at an angle closer to the target surface than the 45° case. This agrees with the phenomenon that the electron energy spectrum contains much more MeV fast electrons in the high energy tail for the 70° case shown in Figure 2.

Note that the preplasma produced at the planar target surface in our experiment expands freely toward the vacuum. The orientation of the preplasma bubble is much different from the preplasma filling in a cone targets (Baton *et al.*, 2008; Van Woerkom *et al.*, 2008). Such difference can lead to different *B* and *E* profiles, resulting in different fast electron transport behaviors.

The main difference between this experiment and our previous one (Li *et al.*, 2006*b*) is that different fast electron groups are investigated. In the previous experiment, the main diagnostic is to measure fast electron angular distributions using imaging plate, which detects the fast electrons escaping from plasma into vacuum, not the electrons transporting and depositing energy in the target. While in this experiment, the main diagnostic is Cu-*Kα* imaging, which is signature of the fast electron transport and energy deposition in the target.

SUMMARY

We have experimentally studied the effect of laser incidence angle on lateral fast electron transport with a preplasma presented. It is shown that when the incidence angle is large (70°), the K_α halo surrounding the laser focus is largely extended to laser propagation direction. Simultaneously, a group of fast electrons with energies of MeV is observed close to the target surface. Simulation results show that the asymmetrical self-generated magnetic field arising from the deformation of the preplasma due to the ponderomotive force is probably responsible for the directional lateral electron transport for large incidence angles.

ACKNOWLEDGMENTS

This work is supported by the National Nature Science Foundation of China (Grants No. 10925421, 10735050, 10974250, 10935002), National Basic Research Program of China (973 Program) (Grant No.2007CB815101) and the National High-Tech ICF program.

REFERENCES

Akli, K.U., Key, M.H., Chung, H.K., Hansen, S.B., Freeman, R.R., Chen, M.H., Gregori, G., Hatchett, S., Hey, D., Izumi, N., King, J., Kuba, J., Norreys, P., Mackinnon, A.J., Murphy, C.D., Snavely, R., Stephens, R.B., Stoeckel, C., Theobald, W. & Zhang, B. (2007). Temperature sensitivity of Cu Kα imaging efficiency using a spherical Bragg reflecting crystal. *Phys. Plasmas* **14**, 023102.

Baton, S.D., Koenig, M., Fuchs, J., Benuzzi-Mounaix, A., Guillou, P., Loupias, B., Vinci, T., Gremillet, L., Rousseaux, C., Drouin, M., Lefebvre, E., Dorchies, F., Fourment, C., Santos, J.J., Batani, D., Morace, A., Redaelli, R., Nakatsutsumi, M., Kodama, R., Nishida, A., Ozaki, N., Norimatsu, T., Aglitskiy, Y., Atzeni, S. & Schiavi, A. (2008). Inhibition of fast electron energy deposition due to preplasma filling of cone-attached targets. *Phys. Plasmas* **15**, 042706.

Beg, F.N., Bell, A.R., Dangor, A.E., Danson, C.N., Fews, A.P., Glinsky, M.E., Hammel, B.A., Lee, P., Norreys, P.A. & Tatarakis, M. (1997). A study of picosecond laser–solid interactions up to 10^{19} W cm^{-2}. *Phys. Plasmas* **4**, 447–457.

Chen, M., Sheng, Z.M. & Zhang, J. (2006*a*). On the angular distribution of fast electrons generated in intense laser interaction with solid targets. *Phys. Plasmas* **13**, 014504.

Chen, M., Sheng, Z.M., Zheng, J., Ma, Y.Y., Bari, M.A., Li, Y.T. & Zhang, J. (2006*b*). Surface electron acceleration in relativistic laser-solid interactions. *Opt. Exp*. **14**, 3093–3098.

Gibbon, P. & Forster, E. (1996). Short-pulse laser – plasma interactions. *Plasma Phys. Contr. Fusion* **38**, 769–793.

Habara, H., Adumi, K., Yabuuchi, T., Nakamura, T., Chen, Z.L., Kashihara, M., Kodama, R., Kondo, K., Kumar, G.R., Lei, L.A., Matsuoka, T., Mima, K. & Tanaka, K.A. (2006). Surface Acceleration of Fast Electrons with Relativistic Self-Focusing in Preformed Plasma. *Phys. Rev. Lett*. **97**, 095004.

Koch, J.A., Aglitskiy, Y., Brown, C., Cowan, T., Freeman, R., Hatchett, S., Holland, G., Key, M., Mackinnon, A., Seely, J., Snavely, R. & Stephens, R. (2003). 4.5- and 8-keV emission and absorption x-ray imaging using spherically bent quartz 203 and 211 crystals. *Rev. Sci. Instr*. **74**, 2130–2135.

Kodama, R., Norreys, P.A., Mima, K., Dangor, A.E., Evans, R.G., Fujita, H., Kitagawa, Y., Krushelnick, K., Miyakoshi, T., Miyanaga, N., Norimatsu, T., Rose, S.J., Shozaki, T., Shigemori, K., Sunahara, A., Tampo, M., Tanaka, K.A., Toyama, Y., Yamanaka, Y. & Zepf, M. (2001). Fast heating of ultrahigh-density plasma as a step towards laser fusion ignition. *Nat*. **412**, 798–802.

Li, C.K., Frenje, J.A., Petrasso, R.D., Seguin, F.H., Amendt, P.A., Landen, O.L., Town, R.P.J., Betti, R., Knauer, J.P., Meyerhofer, D.D. & Soures, J.M. (2009). Pressure-driven, resistive magnetohydrodynamic interchange instabilities in laser-produced high-energy-density plasmas. *Phys. Rev. E* **80**, 016407.

Li, C.K., Seguin, F.H., Frenje, J.A., Rygg, J.R., Petrasso, R.D., Town, R.P.J., Amendt, P.A., Hatchett, S.P., Landen, O.L., Mackinnon, A.J., Patel, P.K., Smalyuk, V.A., Sangster, T.C. & Knauer, J.P. (2006*a*). Measuring E and B Fields in Laser-Produced Plasmas with Monoenergetic Proton Radiography. *Phys. Rev. Lett*. **97**, 135003.

Li, Y.T., Yuan, X.H., Xu, M.H., Zheng, Z.Y., Sheng, Z.M., Chen, M., Ma, Y.Y., Liang, W.X., Yu, Q.Z., Zhang, Y., Liu, F., Wang, Z.H., Wei, Z.Y., Zhao, W., Jin, Z. & Zhang, J. (2006*b*). Observation of a Fast Electron Beam Emitted along the Surface of a Target Irradiated by Intense Femtosecond Laser Pulses. *Phys. Rev. Lett*. **96**, 165003.

Li, Y.T., Zhang, J., Chen, L.M., Mu, Y.F., Liang, T.J., Wei, Z.Y., Dong, Q.L., Chen, Z.L., Teng, H., Chun-Yu, S.T., Jiang, W.M., Zheng, Z.J. & Tang, X.W. (2001). Hot electrons in the interaction of femtosecond laser pulses with foil targets at a moderate laser intensity. *Phys. Rev. E* **64**, 046407.

Lin, X.X., Li, Y.T., Liu, B.C., Liu, F., Du, F., Wang, S.J., Lu, X., Chen, L.M., Zhang, L., Liu, X., Wang, J., Liu, F., Liu, X.L., Wang, Z.H., Ma, J.L., Wei, Z.Y. & Zhang, J. (2010). Effect of prepulse on fast electron lateral transport at the target surface irradiated by intense femtosecond laser pulses. *Phys. Rev. E* **82**, 046401.

Ma, Y.Y., Sheng, Z.M., Li, Y.T., Zhang, J., Yuan, X.H., Xu, M.H., Zheng, Z.Y., Chang, W.W., Chen, M. & Zheng, J. (2006). Preplasma effects on the emission directions of energetic electrons in relativistic laser–solid interactions Journal. *J. Plasma Phys*. **72**, 1269–1272.

Mora, P. & Pellat, R. (1979). Self-similar expansion of a plasma into a vacuum. *Phys. Fluids* **22**, 2300–2304.

Nakamura, T., Kato, S., Nagatomo, H. & Mima, K. (2004). Surface-Magnetic-Field and Fast-Electron Current-Layer Formation by Ultraintense Laser Irradiation. *Phys. Rev. Lett*. **93**, 265002.

Sentoku, Y., Mima, K., Ruhl, H., Toyama, Y., Kodama, R. & Cowan, T.E. (2004). Laser light and hot electron micro focusing using a conical target. *Phys. Plasmas* **11**, 3083–3087.

Sentoku, Y., Ruhl, H., Mima, K., Kodama, R., Tanaka, K.A. & Kishimoto, Y. (1999). Plasma jet formation and magnetic-field generation in the intense laser plasma under oblique incidence. *Phys. Plasmas* **6**, 2855–2861.

Sheng, Z.M., Sentoku, Y., Mima, K., Zhang, J., Yu, W. & Meyer-Ter-Vehn, J. (2000). Angular Distributions of Fast Electrons, Ions, and Bremsstrahlung x/γ-Rays in Intense Laser Interaction with Solid Targets. *Phys. Rev. Lett*. **85**, 5340–5343.

Stamper, J.A., Mclean, E.A. & Ripin, B.H. (1978). Studies of Spontaneous Magnetic Fields in Laser-Produced Plasmas by Faraday Rotation. *Phys. Rev. Lett*. **40**, 1177–1181.

Stamper, J.A., Papadopo., K Sudan, R.N., Dean, S.O., Mclean, E.A. & Dawson, J.M. (1971). Spontaneous Magnetic Fields in Laser-Produced Plasmas. *Phys. Rev. Lett*. **26**, 1012.

Van Woerkom, L., Akli, K.U., Bartal, T., Beg, F.N., Chawla, S., Chen, C.D., Chowdhury, E., Freeman, R.R., Hey, D., Key, M.H., King, J.A., Link, A., Ma, T., Mackinnon, A.J., Macphee, A.G., Offermann, D., Ovchinnikov, V., Patel, P.K., Schumacher, D.W., Stephens, R.B. & Tsui, Y.Y. (2008). Fast electron generation in cones with ultraintense laser pulses. *Phys. Plasmas* **15**, 056304.

Wallace, J.M. (1985). Nonlocal Energy Deposition in High-Intensity Laser-Plasma Interactions. *Phys. Rev. Lett*. **55**, 707–710.

Wilks, S.C., Kruer, W.L., Tabak, M. & Langdon, A.B. (1992). Absorption of ultra-intense laser pulses. *Phys. Rev. Lett*. **69**, 1383–1386.

Yabuuchi, T., Paradkar, B.S., Wei, M.S., King, J.A., Beg, F.N., Stephens, R.B., Nakanii, N., Hatakeyama, M., Habara, H., Mima, K., Tanaka, K.A. & Larsen, J.T. (2010). Transport study of intense-laser-produced fast electrons in solid targets with a preplasma created by a long pulse laser. *Phys. Plasmas* **17**, 060704.

Zhang, J., Li, Y.T., Sheng, Z.M., Wei, Z.Y., Dong, Q.L. & Lu, X. (2005). Generation and propagation of hot electrons in laser-plasmas. *Appl. Phys. B-Lasers Opt*. **80**, 957–971.